NeuroImage: Clinical 35 (2022) 103032

Contents lists available at ScienceDirect

NeuroImage: Clinical

journal homepage: www.elsevier.com/locate/ynicl

Voxel-based analysis of the metabolic asymmetrical and network patterns in hypermetabolism-associated crossed cerebellar diaschisis

Yuankai Zhu [a], Ge Ruan [b], Sijuan Zou [a], Zhaoting Cheng [a], Xiaohua Zhu [a,*]

[a] Department of Nuclear Medicine and PET Center, Tongji Hospital, Tongji Medical College, Huazhong University of Science and Technology, Wuhan 430030, China
[b] Department of Radiology, Hospital, Hubei University, Wuhan 430062, China

ARTICLE INFO

Keywords:
Crossed cerebellar diaschisis
Asymmetry index
Hypermetabolism
Positron emission tomography
Statistical parametric mapping
Metabolic brain network

ABSTRACT

Crossed cerebellar diaschisis (CCD) has been widely investigated in patients with supratentorial hypometabolism, however, the available evidence about the metabolic feature of CCD in patients with contralateral supratentorial hypermetabolism is lacking. This study aimed to assess the metabolic asymmetrical profile, network pattern and predisposing factors for the hypermetabolism-associated CCD, by using voxel-based asymmetry index (AI) and brain network analyses. Seventy CCD positive (CCD+) and 99 CCD negative (CCD-) patients with unilateral supratentorial hypermetabolism were introduced. Among different brain regions with AI_{max} or AI_{min}, striatum & thalamus was accompanied by the highest positive rate of CCD (85.7% or 70.1%, respectively). CCD+ group had significantly greater AI_{max} (median [IQR], 0.62 [0.44–0.84] vs. 0.47 [0.35–0.61]), supratentorial hypermetabolic volume (1183.5 [399.3–3026.8] vs. 386.0 [152.0–1193.0]) and hypometabolic volume (37796.5 [24741.8–53278.0] vs. 3337.0 [1020.0–17193.0]), and lower AI_{min} (−0.85 [-1.05–−0.73] vs. −0.49 [−0.68–−0.35]) compared with CCD- group (all $P < 0.001$). Logistic regression analysis manifested that patients with AI_{min} located at striatum & thalamus were 16.4 times more likely to present CCD than those at frontal lobe (OR = 16.393; 95% CI, 4.463–60.207; $P < 0.001$), and the occurrence of CCD was also associated with AI_{max} (OR = 49.594; 95% CI, 5.519–445.653; $P < 0.001$) and AI_{min} (OR = 3.133×10^{-4}, 95% CI, 1.693×10^{-5}–5.799×10^{-3}, $P < 0.001$). Brain network analysis indicated that the relative hypermetabolism in the contralateral supplementary motor cortex (SMC) and precuneus gyrus were constant in the CCD related patterns. These results demonstrated that the greater AI_{max}, lower AI_{min} and AI_{min} located at striatum & thalamus should be predisposing factors for CCD in patients with unilateral supratentorial hypermetabolism. Relative increased activities in the contralateral SMC and precuneus gyrus might be attributed to a compensatory mechanism for the abnormal brain network related to CCD.

1. Introduction

Crossed cerebellar diaschisis (CCD), firstly reported in cerebral infarction patients, was defined as coupled hypometabolism and hypoperfusion in the cerebellar hemisphere contralateral to the supratentorial lesions (Baron et al., 1981; Sebök et al., 2021). In addition to the ataxic hemiparesis, cerebellar dysfunction within CCD may be involved in the abnormal posture, shoulder subluxation, and impairment of non-motor functions as well (Chang et al., 2017; Hsieh et al., 2020; Inatomi et al., 2021; Kwon et al., 2015; Nishida et al., 2019; Yoshida et al., 2018). Consequently, more extensive investigations are required for the better intervention of CCD and its associated comorbidities.

At present, the determinant factors for the occurrence of CCD remains inconclusive. A large number of studies related to CCD have focused on the patients with supratentorial hypoperfusion or hypometabolism. It was suggested that the presence of CCD was associated with larger infarct volume and greater severity of symptoms (Kang et al., 2017; Wang et al., 2020). Whereas, other studies showed that the asymmetrical magnitude of cerebral perfusion and hypoperfusion volume were the determinants of CCD (Lee et al., 2017; Nocuń et al., 2013). The phenomenon of hyperperfusion/hypermetabolism-associated CCD has been described in patients with epilepsy, glioma, lymphoma and postoperative patients after bypass surgery for moyamoya disease

* Corresponding author at: Department of Nuclear Medicine, Tongji Hospital, Tongji Medical College, Huazhong University of Science and Technology, No. 1095 Jiefang Ave, Wuhan 430030, China.
E-mail address: evazhu@vip.sina.com (X. Zhu).

https://doi.org/10.1016/j.nicl.2022.103032
Received 9 February 2022; Received in revised form 6 April 2022; Accepted 2 May 2022
Available online 6 May 2022

(Hokari et al., 2012; Liu et al., 2018; Nelissen et al., 2006; Teoh et al., 2014; Uchino et al., 2021). Due to the limited number of reported cases, evidence of predisposing factors for hypermetabolism-associated CCD is yet lacking. Besides, hypermetabolic foci were usually accompanied by peripheral and/or remote hypometabolism. It has not been yet investigated whether hypermetabolic or hypometabolic features in these patients are more relevant to the occurrence of CCD.

Asymmetry index (AI) was the most commonly used indicator for evaluating the severity of CCD (Kang et al., 2015; Ma et al., 2022; Sebök et al., 2021; Takahashi and Horiguchi, 2020; Wang et al., 2020). Region or volume of interest (ROI or VOI) can be defined to calculate the AI parameter of supratentorial lesions responsible for CCD (Hou et al., 2021). Drawing the outline of VOI manually, however, has poor repeatability, and is time-consuming and laborious. Although automatic segmentation by using neuromorphometrics atlas is considered to be more objective, no contour of the metabolic abnormality is exactly the same as any standard brain region. Accordingly, AI calculation based on VOI may give rise to controversial results, especially in specific standard brain regions containing both hypermetabolic and hypometabolic lesions. These dilemmas underscore the need for more precise calculation of AI at the voxel level, which has been utilized for the objective localization of the metabolic abnormalities in epilepsy patients (Zhu et al., 2017). To our knowledge, voxel-based analysis of AI has been used for evaluating the asymmetrical profile only in the hypoperfusion-associated CCD, but not in the hyperperfusion- or hypermetabolism-associated CCD (Nocuń et al., 2013).

Under neuropathological state, brain functional networks across the whole brain might be altered in a characteristic pattern (Schindlbeck et al., 2020). And disease related network patterns have been identified in patients with neurodegenerative disorders (Eidelberg, 2009). The determination of CCD related pattern (CCDRP) would be crucial to gain more insight into the pathophysiological foundation for CCD and its associated symptoms.

The study presented herein aimed to assess the metabolic asymmetrical profile, specific CCDRP and predisposing factors for hypermetabolism-associated CCD, by using voxel-based analysis approach in a variety of diseases. In addition, the discrepancies in metabolic asymmetrical pattern and CCDRP expression between CCD positive (CCD+) and CCD negative (CCD-) patients with unilateral supratentorial hypermetabolic lesions were also investigated.

2. Materials and methods

2.1. Subjects

Clinical and image data were retrospectively collected via electronic medical record system and PET/CT database between Jan 2014 to Dec 2021. Patients with unilateral supratentorial hypermetabolic lesion detected by ^{18}F-fluorodeoxyglucose positron emission tomography (^{18}F-FDG PET) imaging were included. Patients were excluded if they had any contralateral brain structural abnormality (including cerebrum and cerebellum) or contralateral supratentorial metabolic abnormality. Another exclusion criterion was that PET image did not cover the entire cerebrum or cerebellum. Finally, 169 patients (75 females; median [IQR] age, 58 [50–67] years) were introduced in this study. In addition, 116 normal brain ^{18}F-FDG PET images of healthy controls (39 females; median [IQR] age, 50 [41–60] years) were extracted from the open source image datasets (Wang et al., 2021).

2.2. Image acquisition and reconstruction

Static PET/CT images were acquired on a clinical PET/CT scanner (Discovery 690 Elite, GE Medical Systems, USA), at 60 min after intravenous injection of ^{18}F-FDG (3.7 MBq/kg). The algorithm of SharpIR + VUE point HD was used for the PET data reconstruction. The matrix size of reconstructed brain PET images was 192 × 192 × 47 with a voxel size of 1.56 × 1.56 × 3.27 mm^3.

2.3. Image analysis

2.3.1. AI parameter images

All reconstructed brain PET images were flipped around the x-axis to create the mirrored PET images. Both raw and flipped PET images were spatially normalized into a homemade symmetric brain template of tissue probability map (TPM) through statistical parametric mapping 12 (SPM12) software package (Welcome Trust Centre for Neuroimaging, London, UK; https://www.fil.ion.ucl.ac.uk/spm), according to the sophisticated protocol (Kurth et al., 2015). These normalized PET data with a voxel size of 1.5 × 1.5 × 1.5 mm^3, were then smoothed using an 8 mm isotropic Gaussian kernel. For the subjects with left supratentorial lesions, AI parameter images were calculated at the voxel level according to the following formula (Didelot et al., 2010; Kurth et al., 2015):

$$AI = (unflipped - -flipped)/[(unflipped + flipped)/2]$$

For the subjects with right supratentorial lesions, the calculation was according to the following formula:

$$AI = (flipped - -unflipped)/[(unflipped + flipped)/2]$$

By this means, all the AI parameters for hypermetabolic lesions were confined to the left side, facilitating the subsequent comparison between CCD+ and CCD- groups. After a second smoothing using an isotropic 4 mm Gaussian kernel, the brain AI parameter images of CCD+ group were compared with those of CCD- group using voxel-wise SPM analysis (AI-SPM) (Didelot et al., 2010; Zhu et al., 2017). Family-wise error (FWE) corrected P value under 0.05 with cluster level above 50 voxels was regarded as statistically significant.

Besides, AI parameter image of each patient was also compared with those of control group using SPM software (Didelot et al., 2010; Zhu et al., 2017). This procedure was conducted to further determine the maximum of AI (AI_{max}), minimum of AI (AI_{min}) and the brain regions of AI_{max} and AI_{min} for each individual patient. Since AI represents the relative FDG uptake compared with that of mirrored brain region, the AI_{max} and AI_{min} located at different brain regions refer to the value of the most asymmetric hypermetabolic and hypometabolic regions, respectively. The higher the AI_{max}, the more significant the extreme value of asymmetric hypermetabolism. In contrast, the lower the AI_{min}, the more significant the extreme value of asymmetric hypometabolism. Both supratentorial hypermetabolic and hypometabolic volumes of all clusters exceeding the threshold were obtained as well.

2.3.2. VOI-based AI

All reconstructed PET images were also spatially normalized to the default TPM template embedded in SPM12 package. VOI for bilateral cerebellum exterior, caudate, putamen, pallidum and thalamus proper, were automatically segmented on both brain hemispheres by the neuromorphometrics atlas matching the default TPM template, and originating from the OASIS project (https://www.oasis-brains.org/). Based on the lateralization of supratentorial lesions, AI for the ipsilateral caudate, putamen, pallidum and thalamus proper was calculated according to the following formula (Takahashi and Horiguchi, 2020):

$$AI = (ipsilateral - -contralateral)/[(ipsilateral + contralateral)/2]$$

But the calculation of AI for the contralateral cerebellum exterior was according to the following formula:

$$AI = (contralateral - -ipsilateral)/[(ipsilateral + contralateral)/2]$$

The determination of CCD was based on the value of cerebellar AI. Patients with cerebellar AI < -0.1 were considered as CCD+, and those with cerebellar AI between $-$ 0.1 and 0.1 as CCD-. None subjects had cerebellar AI exceeding 0.1. Besides, the presence of supratentorial

hypermetabolism were visually evaluated by two experienced nuclear medicine physicians separately. Discordant results were adjudicated by VOI-AI analysis taking 0.1 as the threshold.

2.3.3. Metabolic brain network analysis

Based on the location of supratentorial hypermetabolic lesions, both CCD+ and CCD- patients were classified into 6 categories, i.e. frontal lobe, parietal lobe, temporal lobe, occipital lobe, cingulate gyrus and striatum & thalamus. As described above, brain PET images with right supratentorial lesions were flipped around the x-axis to create the mirrored PET images, thus the hypermetabolic lesions of all images were confined to the left side. Voxel-based metabolic brain network analysis was conducted by scan analysis and visualization processor (ScAnVP) software package (Center for Neuroscience, Feinstein Institute for Medical Research, NY; https://www.feinsteinneuroscience.org). Briefly, CCDRP was determined from the combined control and CCD+ groups for each category, by applying the scaled subprofile model of principal component analysis (SSM-PCA) (Ma et al., 2007). Maximum separation in the expression of CCDRP between the control and CCD+ subjects was achieved, and the principal components expression in each individual case was transformed into Z score. In addition, The CCDRP expressions in the PET data from CCD- subjects calculated through the algorithm of topographic profile rating, were represented by a Z-transformed score as well.

2.4. Statistical analysis

Statistical analyses were conducted by using SPSS software (version 25.0; IBM SPSS Statistics). Group differences for continuous variables were tested using the Mann–Whitney test or Kruskal-Wallis test followed by post-hoc Bonferroni correction, while categorical variables using the chi-square test or Fisher exact test as appropriate. Correlation analyses were performed using Pearson or Spearman correlation coefficients when appropriate. Multivariate logistic regression analysis was conducted to determine the effects of multiple variables on hypermetabolism-associated CCD. P values < 0.05 were considered statistically significant.

3. Results

3.1. The demographics of CCD+ and CCD- groups

CCD was confirmed in 70(41.4%) patients with unilateral supratentorial hypermetabolism. As shown in Table 1, no significant differences in age ($P = 0.494$), gender ($\chi^2 = 1.530$, $P = 0.216$) or lateralization of hypermetabolic lesions ($\chi^2 = 0.120$, $P = 0.729$) were found between CCD+ and CCD- groups. A significant difference in positive rate of hypermetabolism-associated CCD was found among the 5 types of brain disorders (Fisher exact test, $\chi^2 = 12.341$, $P < 0.01$). Without considering the encephalitis with only 1 case, patients with glioma and epilepsy had the highest (63.0%) and lowest (0%) positive rate of CCD, respectively.

3.2. Comparison of metabolic asymmetrical pattern between CCD+ and CCD- groups

Compared with CCD- group, no significant increase of metabolic AI was found in CCD+ group ($P_{[FWE\text{-}corrected]} < 0.05$, cluster size > 50). Whereas, CCD+ group had significantly lower metabolic AI mainly in ipsilateral thalamus, insula, inferior frontal gyrus and pons and contralateral cerebellum than CCD- group ($P_{[FWE\text{-}corrected]} < 0.05$, cluster size > 50; Fig. 1 and Table 2). Only 3 local maxima >8 mm apart were displayed for each cluster in Table 2. Besides, significant reduction of metabolic AI was also found in ipsilateral frontal lobe (33740 voxels), parietal lobe (7377 voxels), temporal lobe (5584 voxels), putamen (2213 voxels), caudate (1051 voxels), pallidum (478 voxels) and midbrain (723 voxels) including the red nucleus (75 voxels).

Table 1
The demographics of patients with unilateral supratentorial hypermetabolism.

Clinical characteristics	CCD+ group (n = 70)	CCD- group (n = 99)	P value	χ^2
Gender				
Female/Male	35/35	40/59	0.216	1.530#
Age (years)	59 (50–68)	58 (49–67)	0.494	N/A
Lateralization (L/R)	37/33	55/44	0.729	0.120#
Disease category			0.008	12.341*
Epilepsy	0	8		
Glioma	17	10		
Lymphoma	8	9		
Metastatic tumor	45	71		
Encephalitis	0	1		
Region with AI_{max}			0.016	13.564*
Frontal lobe	40	43		
Parietal lobe	7	21		
Temporal lobe	7	18		
Occipital lobe	5	12		
Insula & cingulate gyrus	5	4		
Striatum & thalamus	6	1		
Region with AI_{min}			<0.001	38.634*
Frontal lobe	13	36		
Parietal lobe	6	20		
Temporal lobe	3	18		
Occipital lobe	1	3		
Insula & cingulate gyrus	0	2		
Striatum & thalamus	47	20		

AI = asymmetry index; CCD = crossed cerebellar diaschisis; L = left cerebral hemisphere; R = right cerebral hemisphere; # Pearson chi-square test; * Fisher exact test.

3.3. Analysis of the individual metabolic asymmetrical profile for hypermetabolism-associated CCD

Compared with control group, individual metabolic asymmetrical profile of each patient (both CCD+ and CCD- group) with unilateral supratentorial hypermetabolism was analyzed, in order to obtain asymmetrical parameters including AI_{max}, AI_{min}, brain region with AI_{max} or AI_{min}, and volume of supratentorial hypermetabolism or hypometabolism. The metabolic asymmetrical profile of a single CCD+ patient with glioma was demonstrated as an example in Fig. 2 and Table 3 ($P_{[FWE\text{-}corrected]} < 0.05$, cluster size > 50).

As shown in Table 1, significant difference in positive rate of CCD was found among 6 brain regions with AI_{max} (Fisher exact test, $\chi^2 = 13.564$, $P < 0.05$), as well as regions with AI_{min} (Fisher exact test, $\chi^2 = 38.634$, $P < 0.001$). Among different brain regions with AI_{max} or AI_{min}, striatum & thalamus was accompanied by the highest positive rate of CCD (85.7% or 70.1%, respectively). In addition, CCD+ group had significantly greater AI_{max} (median [IQR], 0.62 [0.44–0.84] vs. 0.47 [0.35–0.61], $P < 0.001$), supratentorial hypermetabolic volume (median [IQR], 1183.5 [399.3–3026.8] vs. 386.0 [152.0–1193.0], $P < 0.001$) and hypometabolic volume (median [IQR], 37796.5 [24741.8–53278.0] vs. 3337.0 [1020.0–17193.0], $P < 0.001$) compared with CCD- group (Fig. 3). AI_{min} of CCD+ group was significantly lower than that of CCD- group (median [IQR], −0.85 [-1.05–−0.73] vs. −0.49 [−0.68–−0.35], $P < 0.001$).

Both the volume ratio of hypometabolism to hypermetabolism (median [IQR], 35.36 [8.39–121.11] vs. 7.66 [2.08–35.57], $P < 0.001$) and the total volume of metabolic abnormalities (median [IQR], 40318.5 [26090.0–55456.0] vs. 5177.0 [1545.0–19352.0], $P < 0.001$) of CCD+ group were significantly greater than those of CCD- group. Furthermore, significant difference in the volume ratio of hypometabolism to hypermetabolism ($P = 0.007$), as well as in the total volume of metabolic abnormalities ($P = 0.001$), were found among the 4

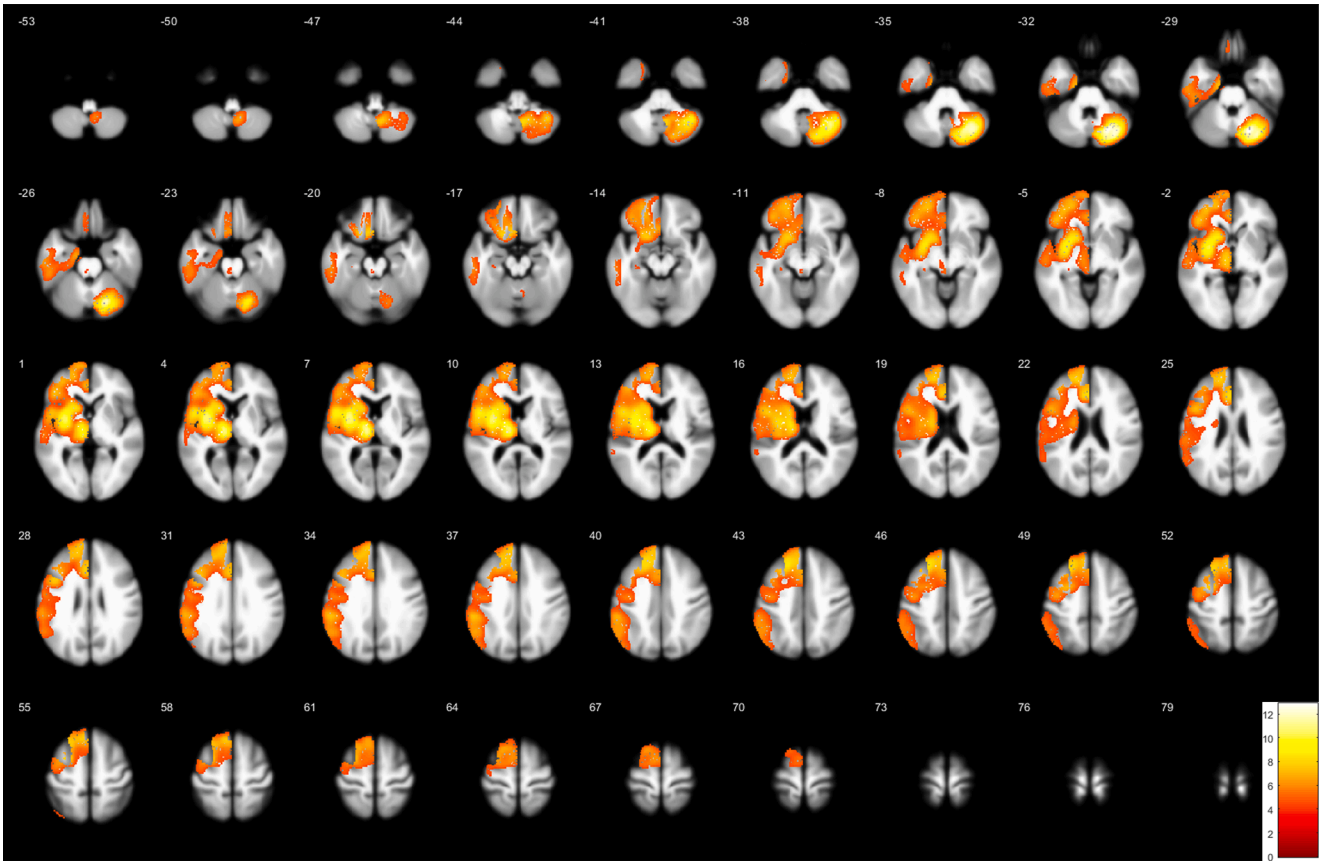

Fig. 1. The decreased metabolic asymmetrical profile of CCD+ patients compared with CCD- patients. Raw PET images were flipped around the x-axis to create the mirrored images, resulting all the hypermetabolic lesions confined to the left side. The brain metabolic AI parameter images of CCD+ group were compared with those of CCD- group using voxel-wise SPM analysis. Family-wise error corrected *P* value under 0.05 with cluster level above 50 voxels was regarded as statistically significant. See also Table 2.

Table 2
The decreased metabolic asymmetrical profile of CCD+ patients compared with CCD- patients.

Clusters			Peak level		Coordinates (mm)			Regions
	K_E	*P* (FWE-corrected)	*P* (FWE-corrected)	T	X	Y	Z	
1	9519	0.000	0.000	12.87	21	−70	−30	Cerebellum (contralateral)
			0.000	12.24	32	−75	−31	Cerebellum (contralateral)
			0.000	8.05	8	−58	−45	Cerebellum (contralateral)
2	67,285	0.000	0.000	11.01	−11	−16	7	Thalamus (ipsilateral)
			0.000	10.74	−33	2	7	Insula (ipsilateral)
			0.000	9.05	−48	7	7	OpIFG (ipsilateral)
3	62	0.020	0.019	4.54	−3	31	−24	Pons (ipsilateral)

Table showing 3 local maxima>8 mm apart in each cluster; CCD = crossed cerebellar diaschisis; K_E = cluster size; FWE = Family-wise error; FDR = False discovery rate; OpIFG = opercular part of the inferior frontal gyrus. See also Fig. 1.

types of brain disorders (excluding the only one encephalitis patient). The post hoc analysis indicated that the volume ratio of hypometabolism to hypermetabolism in both glioma (median [IQR], 21.45 [6.80–56.42], $P = 0.023$) and metastatic tumor (median [IQR], 20.49 [5.14–75.15], $P = 0.009$) patients, was significantly greater than that in epilepsy patients (median [IQR], 2.31 [0.14–4.71]), while the total volume of metabolic abnormalities in both metastatic tumor (median [IQR], 18973.5 [2907.3–40697.0] $P = 0.022$) and epilepsy (median [IQR], 5450.0 [975.3–12849.0], $P = 0.002$) patients was significantly lower than that in glioma patients (median [IQR], 34155.0 [18846.0–55756.0]).

Logistic regression analysis was performed with relevant factors, including disease category, AI_{max}, AI_{min}, region with AI_{max}, region with AI_{min}, supratentorial hypermetabolic and hypometabolic volumes, volume ratio of hypometabolism to hypermetabolism and total volume of metabolic abnormalities, which were significantly different between CCD+ and CCD- groups in the univariate analysis. Patients with AI_{min} located at striatum & thalamus were 16.4 times more likely to present hypermetabolism-associated CCD than those at frontal lobe (odds ratio [OR] = 16.393; 95% CI, 4.463–60.207; $P < 0.001$, Table 4). The occurrence of CCD was also significantly associated with the values of AI_{max} (OR = 49.594; 95% CI, 5.519–445.653; $P < 0.001$) and AI_{min} (OR = 3.133×10^{-4}, 95% CI, 1.693×10^{-5}–5.799×10^{-3}, $P < 0.001$).

3.4. Correlation between metabolic AI of ipsilateral striatum & thalamus and that of contralateral cerebellum

Among CCD+ group, metabolic AI of contralateral cerebellum was significantly positively correlated with that of ipsilateral caudate,

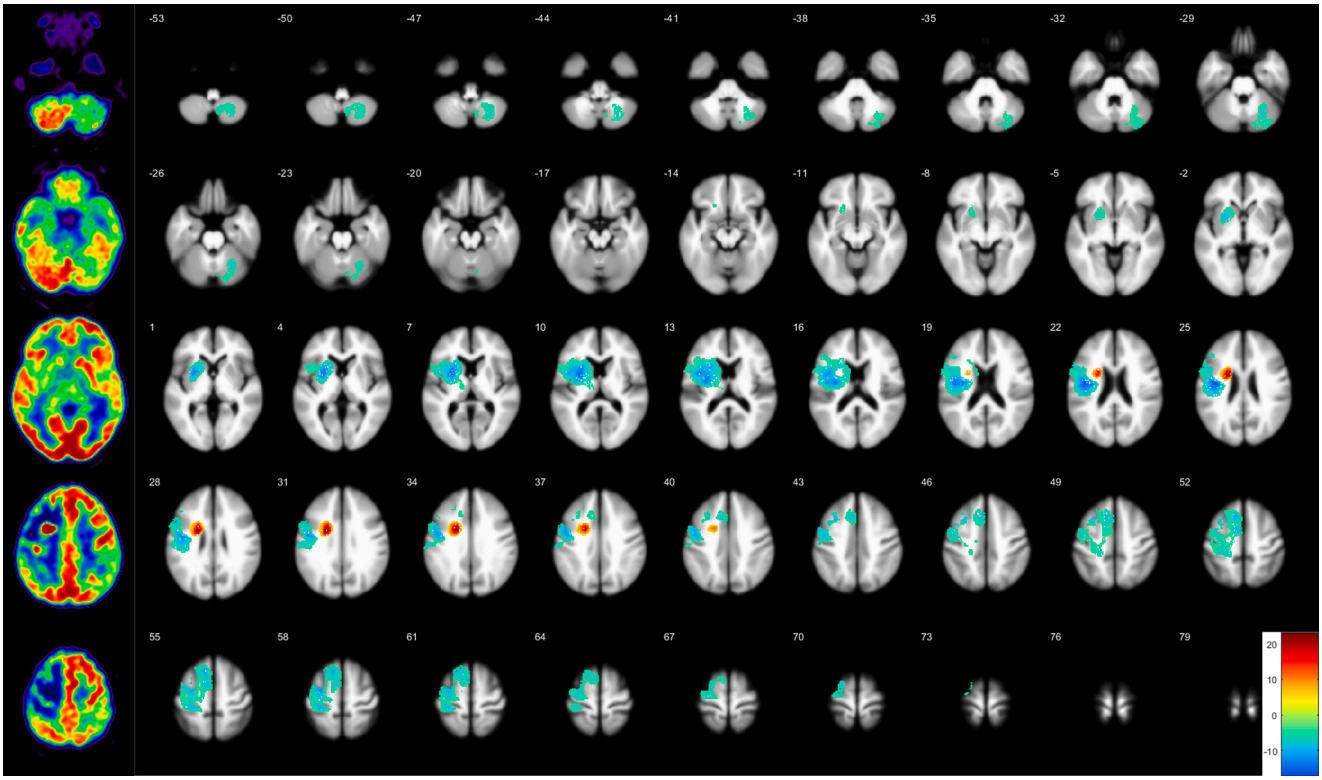

Fig. 2. The interhemispheric metabolic asymmetrical profile of a single CCD+ patient with left supratentorial glioma. Family-wise error corrected *P* value under 0.05 with cluster level above 50 voxels was regarded as statistically significant. Regions with increased metabolic AI were in yellow/red, reduced metabolic AI in blue/green. See also Table 3. (For interpretation of the references to color in this figure legend, the reader is referred to the web version of this article.)

Table 3
The metabolic asymmetrical profile of a glioma patient with hypermetabolism-associated CCD.

Clusters	Cluster level		Peak level		Coordinates (mm)			Regions
	K_E	*P* (FWE-corrected)	*P* (FWE-corrected)	T	X	Y	Z	
Increased								
1	1715	0.000	0.000	22.87	−21	2	31	Frontal lobe (ipsilateral)
Decreased								
1	22,558	0.000	0.000	16.99	−41	−9	23	Frontal lobe (ipsilateral)
			0.000	15.11	−27	4	8	Putamen (ipsilateral)
			0.000	13.64	−30	−7	14	Insula (ipsilateral)
2	4077	0.000	0.000	8.08	11	−58	−57	Cerebellum (contralateral)
			0.000	8.08	27	−64	−28	Cerebellum (contralateral)
			0.000	7.48	33	−81	−30	Cerebellum (contralateral)
3	51	0.004	0.000	6.86	−47	31	25	Frontal lobe (ipsilateral)
4	58	0.003	0.002	5.55	6	−73	−25	Cerebellum (contralateral)

Table showing 3 local maxima>8 mm apart in each cluster; CCD = crossed cerebellar diaschisis; K_E = cluster size; FWE = Family-wise error; FDR = False discovery rate. See also Fig. 2.

putamen, pallidum and thalamus proper (r = 0.317, 0.333, 0.345 and 0.373, respectively, all $P < 0.01$; Fig. 4). Whereas among CCD- group, metabolic AI of contralateral cerebellum was significantly positively correlated only with that of ipsilateral caudate (r = 0.252, $P < 0.05$) and putamen ($r_s = 0.339$, $P < 0.01$).

3.5. Metabolic brain network analysis for hypermetabolism-associated CCD

Since hypermetabolic lesion located at insula lobe was found only in 1 CCD+ subject, this subject was not included in the establishment of CCDRP. Hypermetabolism-associated CCDRP was determined for each category based on the location of supratentorial hypermetabolic lesions (Fig. 5).

The frontal lobe associated CCDRP accounting for 40.02% of the subject × voxel variance, was characterized by relative increases in contralateral supplementary motor cortex (SMC) and precuneus gyrus (PrG) metabolism, associated with relative reductions in ipsilateral frontal lobe, insula lobe, caudate, putamen, anterior cingulate gyrus and contralateral cerebellum (Fig. 5a). The parietal lobe associated CCDRP accounting for 20.57% of the subject × voxel variance, was characterized by relative increases in contralateral SMC, PrG, precentral gyrus and postcentral gyrus metabolism, associated with relative reductions in ipsilateral parietal lobe, frontal lobe, temporal lobe, occipital lobe, cingulate gyrus, insula lobe, thalamus and contralateral cerebellum (Fig. 5b). The temporal lobe associated CCDRP accounting for 23.82% of

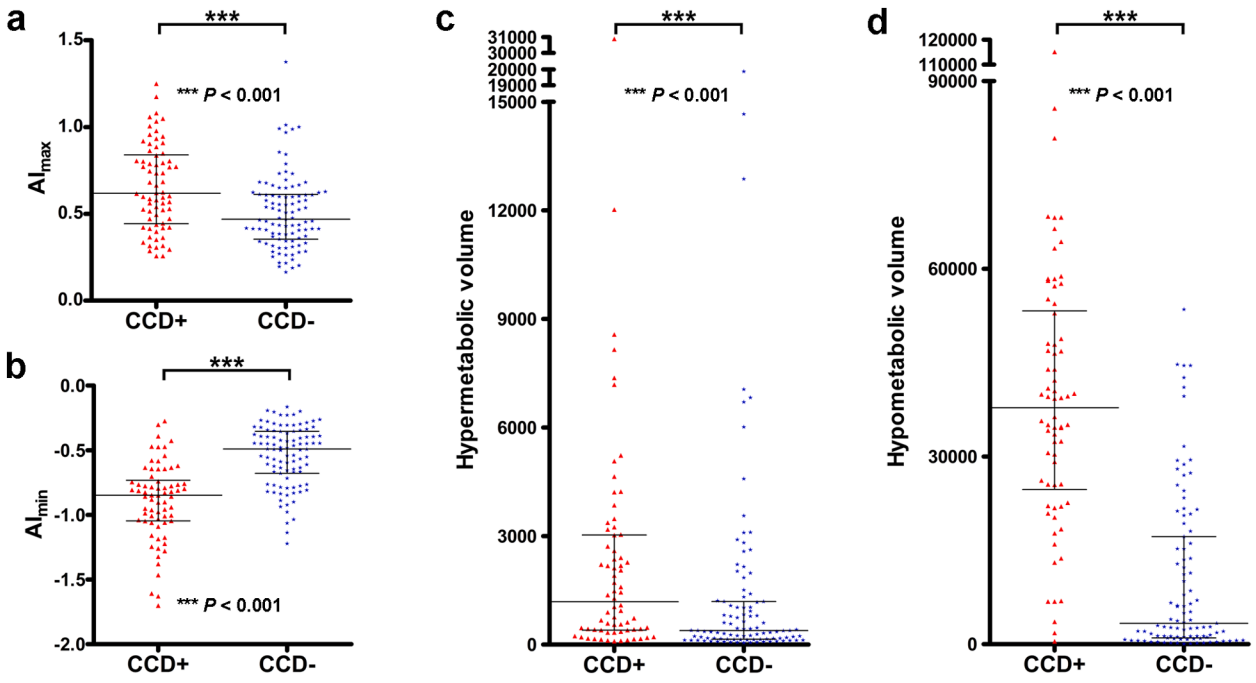

Fig. 3. Comparison of metabolic asymmetrical parameters between CCD+ and CCD- groups. These asymmetrical parameters were derived from the individual AI-SPM analysis. (a) CCD+ group had significantly greater AI_{max} compared with CCD- group (median [IQR], 0.62 [0.44–0.84] vs. 0.47 [0.35–0.61], $P < 0.001$); (b) AI_{min} of CCD+ group was significantly lower than that of CCD- group (median [IQR], −0.85 [−1.05–−0.73] vs. −0.49 [−0.68–−0.35], $P < 0.001$). (c) CCD+ group had significantly larger supratentorial hypermetabolic volume compared with CCD- group (median [IQR], 1183.5 [399.3–3026.8] vs. 386.0 [152.0–1193.0], $P < 0.001$); (d) Supratentorial hypometabolic volume of CCD+ group was significantly larger than that of CCD- group (median [IQR], 37796.5 [24741.8–53278.0] vs. 3337.0 [1020.0–17193.0], $P < 0.001$).

Table 4
Logistic regression analysis of risk factors for hypermetabolism-associated CCD.

Variables	*P*	β	SEM	Exp(β)	95% CI
AI_{max}	<0.001	3.904	1.120	49.594	5.519–445.653
AI_{min}	<0.001	−8.068	1.489	3.133×10^{-4}	1.693×10^{-5}–5.799×10^{-3}
Region with AI_{min}	<0.001				
Frontal lobe	N/A	N/A	N/A	1.000	N/A
Parietal lobe	0.199	−1.072	0.834	0.342	0.067–1.756
Temporal lobe	0.542	0.747	1.225	2.112	0.191–23.309
Occipital lobe	0.191	−1.896	1.451	0.150	0.009–2.580
Insula & cingulate gyrus	1.000	−46.821	9.143×10^{10}	4.635×10^{-21}	N/A
Striatum & thalamus	<0.001	2.797	0.664	16.393	4.463 – 60.207
Constant	<0.001	−9.525	1.655	7.299×10^{-5}	N/A

AI = asymmetry index; CCD = crossed cerebellar diaschisis.

the subject × voxel variance, was characterized by relative increases in contralateral SMC and PrG metabolism, associated with relative reductions in ipsilateral temporal lobe, occipital lobe, insula lobe, putamen, pallidum, thalamus and contralateral cerebellum (Fig. 5c). The occipital lobe associated CCDRP accounting for 17.40% of the subject × voxel variance, was characterized by relative increases in contralateral SMC, PrG, precentral gyrus and postcentral gyrus metabolism, associated with relative reductions in ipsilateral occipital lobe, parietal lobe, temporal lobe, insula lobe, putamen, pallidum, thalamus and contralateral cerebellum (Fig. 5d). The cingulate gyrus associated CCDRP accounting for 18.01% of the subject × voxel variance, was characterized by relative increases in contralateral SMC and superior temporal gyrus metabolism, associated with relative reductions in ipsilateral parietal lobe, cingulate gyrus, frontal lobe, occipital lobe, temporal lobe and contralateral cerebellum (Fig. 5e). And the striatum & thalamus associated CCDRP accounting for 14.83% of the subject × voxel variance, was characterized by relative increases in ipsilateral putamen, pallidum, thalamus and contralateral frontoparietal lobes (including SMC and PrG) metabolism, associated with relative reductions in ipsilateral frontal lobe, parietal lobe, occipital lobe, insula lobe, temporal lobe and contralateral cerebellum (Fig. 5f).

Significant differences in the CCDRP expressions represented by subject Z scores were found among control, CCD+ and CCD- groups, for each category based on the location of supratentorial hypermetabolic lesions (all $P < 0.01$), and the Bonferroni multiple comparisons were shown in Fig. 6. CCD+ group had significantly higher pattern expressions than control group for each category (all $P < 0.01$). CCD- group had significantly higher pattern expressions than control group, for the frontal lobe (Fig. 6a), parietal lobe (Fig. 6b), temporal lobe (Fig. 6c) or occipital lobe (Fig. 6d) associated CCDRP (all $P < 0.001$). No significant difference in the CCDRP expression was found between control and CCD- groups for the cingulate gyrus associated CCDRP (Fig. 6e, $P = 1.000$). Besides, CCD- group had significantly lower pattern expressions than CCD+ group only for the frontal lobe associated CCDRP (Fig. 6a, $P < 0.01$). No significant difference in the CCDRP expression was found between CCD+ and CCD- groups, for the parietal lobe (Fig. 6b, $P = 0.539$), temporal lobe (Fig. 6c, $P = 0.210$), occipital lobe (Fig. 6d, $P = 1.000$) or cingulate gyrus associated CCDRP (Fig. 6e, $P = 0.111$).

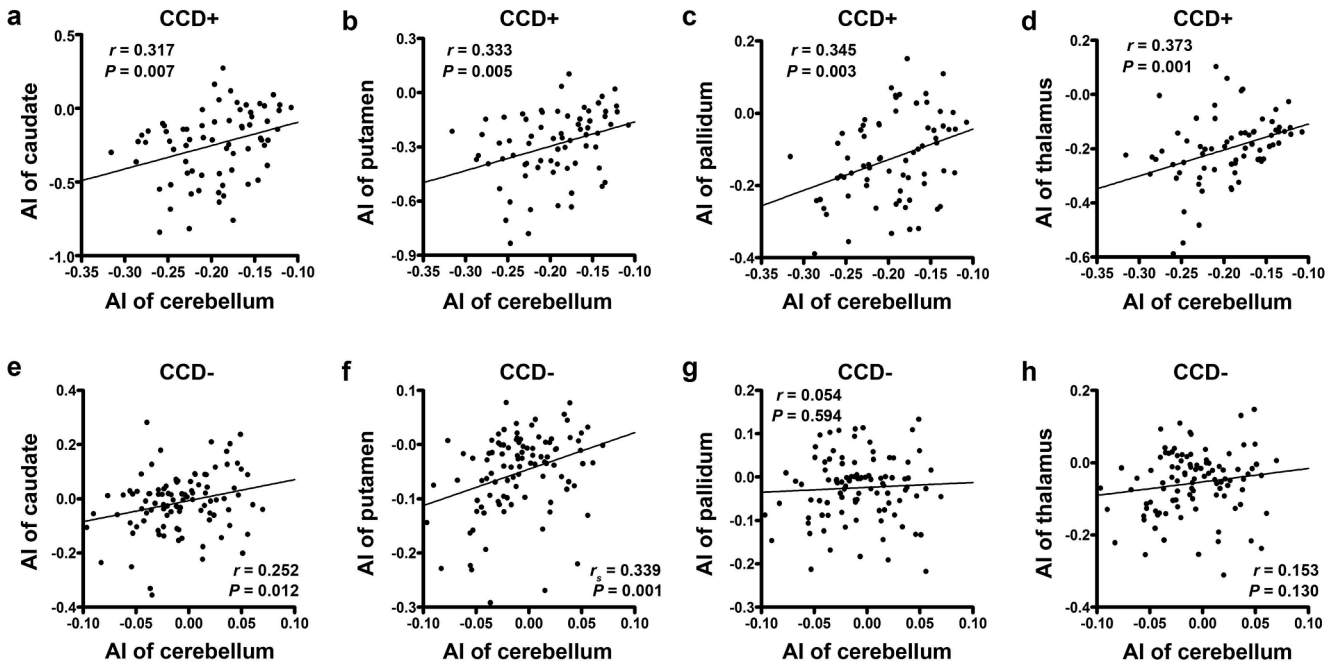

Fig. 4. Correlation between metabolic AI of contralateral cerebellum and that of ipsilateral striatum & thalamus. Metabolic AI of contralateral cerebellum was significantly positively correlated with that of ipsilateral caudate (a), putamen (b), pallidum (c) and thalamus proper (d) among CCD+ patients (all $P < 0.01$), and with that of ipsilateral caudate (e) and putamen (f) among CCD- patients (both $P < 0.05$). No significant correlation was found between metabolic AI of contralateral cerebellum and that of ipsilateral pallidum (e) and thalamus proper (f) among CCD- patients (both $P > 0.05$).

4. Discussion

The current study demonstrated the involvement of both metabolic AI_{max} and AI_{min} in the hypermetabolism-associated CCD by using voxel-based AI analysis approach. Besides, Patients with AI_{min} located at striatum & thalamus were prone to present CCD. Functional connectivities between ipsilateral striatum & thalamus and contralateral cerebellum in CCD+ patients were distinct from those in CCD- patients. Brain network analysis indicated that the relative hypermetabolism in the contralateral SMC and PrG were constant in all the identified CCDRPs.

VOI-based AI was one of the most commonly used indicators for evaluating the severity of CCD (Kang et al., 2015; Ma et al., 2022; Sebök et al., 2021; Takahashi and Horiguchi, 2020; Wang et al., 2020). The VOI can be drawn manually, but the precise definition of the boundary for the metabolic abnormality in functional images is difficult. Therefore, this time-consuming and laborious approach has poor repeatability in the AI analysis for PET images. Although automatic segmentation by using stereotype VOI is considered to be more objective, metabolic abnormality is in a nonuniform distribution and its contour cannot be exactly overlapped with any recognized standard brain region. In particular, the hypermetabolic lesion with small volume may not be detected due to the dilution by peripheral hypometabolism. In order to estimate the location, direction and magnitude of brain morphological asymmetries more precisely, standard guideline for the voxel-based AI analysis protocol was established (Kurth et al., 2015). Very little research attempted to apply this approach for the localization of epileptic foci using PET imaging (Didelot et al., 2010; Zhu et al., 2017). To the best of our knowledge, not considering the conventional SPM procedure, voxel-based AI analysis approach has been used for capturing the asymmetrical profile of brain perfusion only in hypoperfusion-associated CCD using single photon imaging, and it was utilized in the assessment of hypermetabolism-associated CCD for the first time in our study (Nocuń et al., 2013). Above all, greatest advantage of this approach lies in that relatively small volume of hypermetabolic lesions surrounded by widespread hypometabolism (e.g., Fig. 2) would not be detected through VOI-based AI approach.

Up to 70 of 169 (41.4%) patients presented hypermetabolism-associated CCD in our retrospective study. Significant difference in positive rate of CCD was found among different types of brain diseases, which was in line with other studies (7.5% to 57.4%) focused on unilateral supratentorial lesions with reduced metabolism/perfusion only (Franceschi et al., 2021; Hertel et al., 2021; Hou et al., 2021; Ma et al., 2022; Provost et al., 2021; Sebök et al., 2021; von Bieberstein et al., 2021; Zhang et al., 2019). Hypermetabolism-associated CCD was observed in 18.4% of moyamoya disease patients with postoperative cerebral hyperperfusion, and in 26.3% of glioma patients (Sebök et al., 2020; Uchino et al., 2021). Whereas, a majority of CCD studies on supratentorial hypermetabolic lesions were merely exhibited in the form of case report (Calabria and Schillaci, 2012; Goldwaser et al., 2020; Hokari et al., 2012; Teoh et al., 2014). In the current study, it was suggested that patients with unilateral supratentorial glioma were more likely (63.0%) to suffer from hypermetabolism-associated CCD, and had larger total volume of metabolic abnormalities compared with patients with unilateral supratentorial metastatic tumor. The possible reason may be that the AI of cerebellar perfusion/metabolism was related with the total supratentorial lesion volume, including not only the tumor but also the peritumoral edema (Liu et al., 2018). Apart from the peritumoral notable edema, remote inhibition induced by the interruption of nervous pathways could further increase the volume of reduced perfusion/metabolism (Lindegaard et al., 1986; Nelissen et al., 2006). Since there was hardly any other available evidence for the discrepancy in the susceptibility to CCD among multiple types of brain disorders, more researches are needed to explore this disparity.

Surprisingly in this study, no hypermetabolism-associated CCD was detected in any epilepsy patients. Among refractory epilepsy patients caused by focal cortical dysplasia, 23.0% of them presented CCD with unilateral supratentorial hypometabolic lesions (Hou et al., 2021). The larger range of supratentorial hypometabolism, detectable structural abnormalities and the AI_{min} located at the posterior frontal & anterior temporal lobes, were considered as predisposing factors for the occurrence of CCD in epilepsy patients (Hou et al., 2021; Savic et al., 1996). In

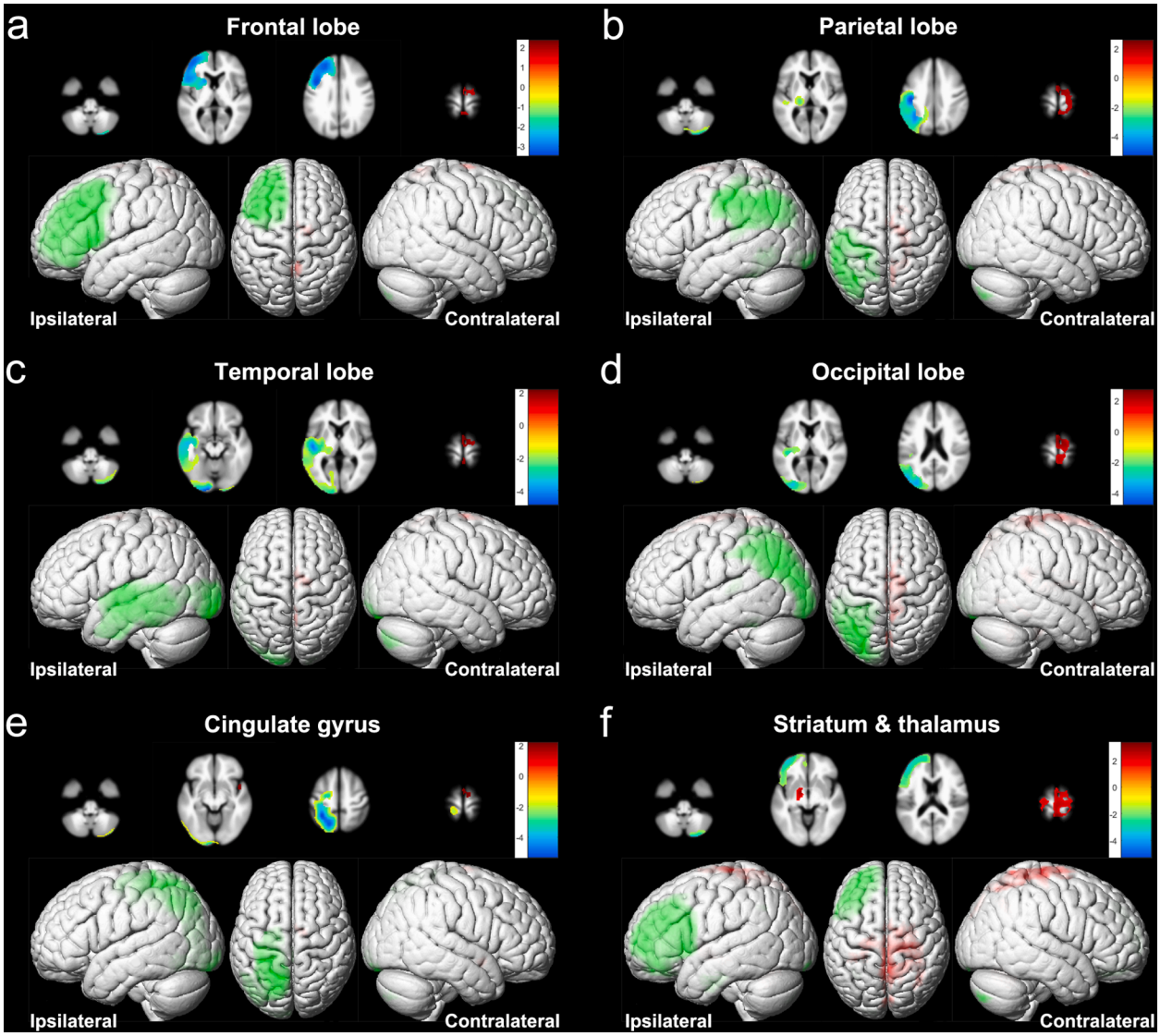

Fig. 5. Metabolic brain network analysis for hypermetabolism-associated CCD. CCD-related patterns were identified in patients with unilateral supratentorial hypermetabolic lesions, located at frontal lobe (a), parietal lobe (b), temporal lobe (c), occipital lobe (d), cingulate gyrus (e) and striatum & thalamus (f), respectively. In the render view, voxels with increased metabolism is displayed in red color, while those with decreased metabolism in green color. (For interpretation of the references to color in this figure legend, the reader is referred to the web version of this article.)

addition, hypometabolism-associated CCD was found in 22.2% epilepsy patients with Sturge-Weber syndrome as well, and occurred more frequently (81%) in the interventional test (Griffiths et al., 1997; Kurthen et al., 1990). However, within our knowledge, canonical contralateral cerebellar hypometabolism in epilepsy patients with unilateral supratentorial hypermetabolic lesions has not been reported. Put another way, contralateral cerebellar hyperperfusion/hypermetabolism (CCH) may be the characteristic form of reverse CCD in certain epilepsy patients (Graffeo et al., 2016; Park et al., 1992; Won et al., 2018; Yokota and Ida, 2019). This interesting phenomenon was exclusively observed in the ictal state or status epilepticus, and could convert into conventional CCD or symmetrical pattern after seizure were controlled (Cui et al., 2014; Goldwaser et al., 2020; Kawai et al., 2005; Umemura and Suzuka, 2000). Accompanied by the vascular dilatation and increased perfusion, neuronal hyperactivation may be attributed to the widespread epileptiform discharges and prolonged excitatory synaptic activities via cortico-ponto-cerebellar pathway (Koy et al., 2012; Vyas et al., 2019).

CCD, a condition in opposition to CCH, was considered to arise from the deafferentation of cortico-ponto-cerebellar pathway (Reesink et al., 2018). Along this pathway, CCD+ group had significantly lower metabolic AI within ipsilateral cerebral cortex (excluding occipital lobe), cerebral white matter, pons and contralateral cerebellum compared with CCD- group in our voxel-based AI analysis. It was suggested that both the magnitude of declined metabolism and the total supratentorial hypometabolic volume may be predisposing factors for CCD (Hou et al., 2021; Lee et al., 2017; Sommer et al., 2016). Thus, we speculated that the sufficiently low AI_{min} and large volume of supratentorial hypometabolism in CCD+ patients could allow the cortico-ponto-cerebellar pathway to be suppressed. Furthermore, our results revealed that the magnitude of elevated metabolism (AI_{max}) in brain lesions might also be related to the presence of CCD in patients with supratentorial hypermetabolism. The excessive supratentorial dysfunction could further inhibit the activity of ipsilateral pons, the relay station of this pathway, through the intrahemispheric associative neurofibrillary tangles. Eventually, the apparent decline of metabolic activity in ipsilateral pons may induce the presence of CCD, accompanied by the reduced neurological activities in the downstream contralateral cerebellum.

Interestingly, apart from the hypometabolism of the entire cortico-ponto-cerebellar pathway delineated in our AI-SPM analysis,

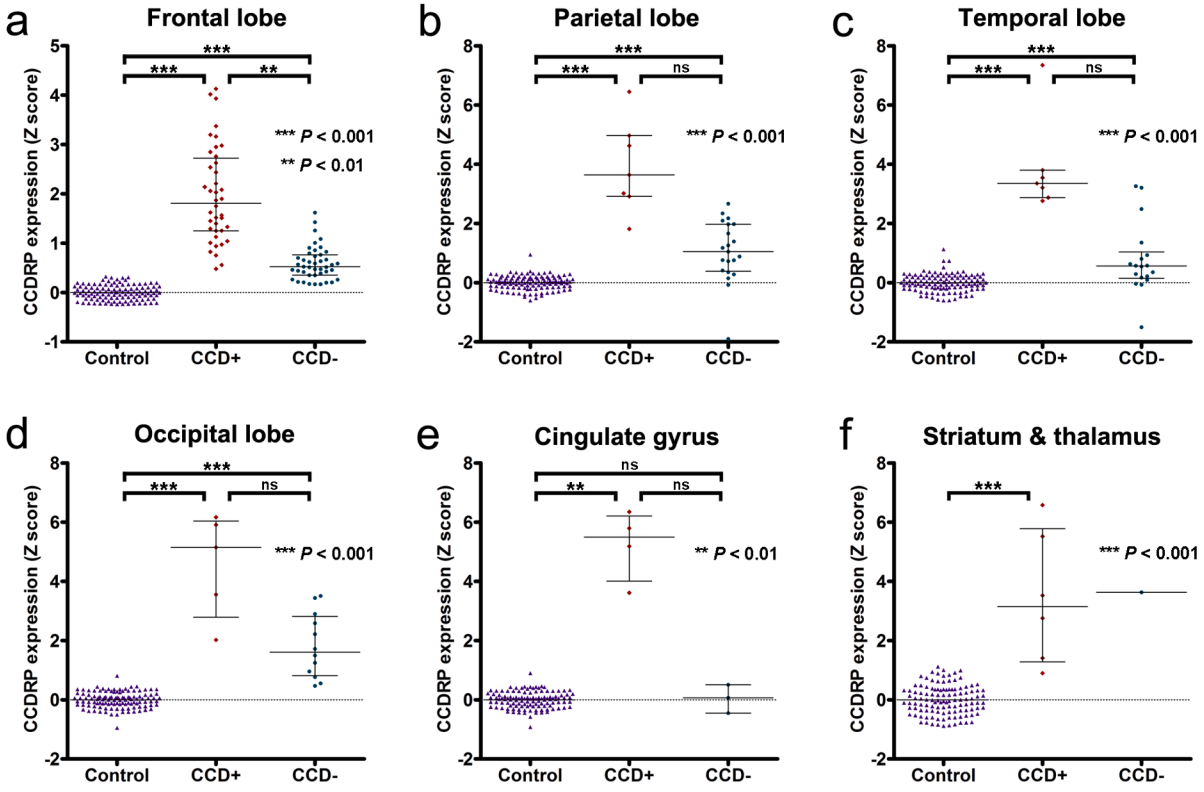

Fig. 6. Comparison of CCD-related pattern (CCDRP) expressions among control, CCD+ and CCD- groups. Individual Z scores (pattern expressions of CCDRP) in CCD- group with unilateral supratentorial hypermetabolic lesions located at frontal lobe (a), parietal lobe (b), temporal lobe (c), occipital lobe (d), cingulate gyrus (e) and striatum & thalamus (f), respectively, were compared with those in control and CCD+ groups.

ipsilateral striatum, thalamus and red nucleus were also detected with declined metabolism in hypermetabolism-associated CCD. These subcortical nuclei are the key components of cortico-rubral pathway. The inhibition of this pathway would further lead to the dysfunction of successive rubro-spinal tract, resulting the symptom of hemiataxia. Logistic regression analysis also indicated that AI_{min} located at striatum & thalamus should be a pivotal predisposing factor for hypermetabolism-associated CCD, which was in accordance with the researches on hypometabolism-associated CCD (Chen et al., 2014; Lin et al., 2018; Noguchi et al., 2015; Sin et al., 2018). The neighboring internal capsule with compact fiber bundle may also be involved, inducing the inhibition of the cortico-ponto-cerebellar pathway. Moreover, striatum and thalamus were also considered to be involved in the process of cognitive function (Diehl-Schmid et al., 2019; Hirata et al., 2015; Leisman and Melillo, 2013). These findings may provide a new insight into not only the hemiataxia, but also the cognitive and behavior comorbidities of CCD (Devita et al., 2021; Leisman and Melillo, 2013).

In our VOI-based AI analysis, the correlation between contralateral cerebellar cortex and ipsilateral striatum and thalamus were appraised in both CCD+ and CCD- patients. The metabolic activity of contralateral cerebellum was positively correlated with that of ipsilateral striatum and thalamus in CCD+ patients, but with that of only ipsilateral neostriatum in CCD- patients. The complex interactive functional network with reciprocal communication between cerebellum and basal ganglia has been verified (Bostan et al., 2013). It was also indicated that the subthalamic nucleus was the key node of the efferent projection from the basal ganglia to the cerebellum (Bostan et al., 2010). The cerebellum influenced the striatal process by the dentate nucleus (Hoshi et al., 2005). Besides, the efferent projections from the cerebellum to both contralateral cerebral cortex and basal ganglia were relayed via thalamus, influencing multiple motor and cognitive functions (Hamaide et al., 2018; Kawabata et al., 2020; Palesi et al., 2017). Therefore, we speculated that the synchronously reduced activities of ipsilateral striatum & thalamus and contralateral cerebellum could be related to the hypermetabolism-associated CCD and its symptoms.

Distinct CCDRPs were determined based on the category for the location of supratentorial hypermetabolic lesions in our study. However, the relative metabolic increases in the contralateral SMC and PrG, especially the SMC, were constant in all the established patterns. The area of SMC was supposed to be critical for the learning, execution and regulation of motor action (Bonini et al., 2014). Other non-motor functions including auditory processing, cognitive control, apraxia, and aphasia also involve the participation of SMC (Joswig et al., 2021; McGettigan et al., 2013; Sjöberg et al., 2019; Yajima and Naruse, 2021). In addition, neuroimaging evidences revealed that PrG along with its cortical and subcortical connectivity could regulate not only the motor function, but also the higher-order cognitive function, e.g., visuo-spatial imagery, memory and conscious (Cavanna and Trimble, 2006; Thibes et al., 2017). Considering the CCD associated motor and non-motor symptoms, these increased activities in contralateral SMC and PrG might be attributed to a compensatory mechanism for abnormal brain function.

Though the network pattern expressions in CCD- subjects were significantly higher than those in control group, both of them failed to reach the expression level in CCD+ subjects, for those with hypermetabolic lesion located at frontal lobe. Therefore, the expression of the established CCDRP, has the potential to distinguish the CCD- group from both control and CCD+ groups. The unexpected finding was that no significant difference in the CCDRP expression was found between CCD+ and CCD- groups, for those with hypermetabolic lesion outside the frontal area. Owing to the limited number of CCD+ subjects in these categories, the network patterns were potentially unstable, which would be a possible explanation. Further investigation with a larger sample size could provide a more convincing CCDRP, in order to develop more

effective therapies targeting the key brain regions or pathways responsible for CCD.

Due to the limitation of the experimental design, numerous patients with bilateral supratentorial hypermetabolic lesions, mostly brain metastatic tumor, and glioma patients without obvious hypermetabolic lesions were excluded from this study. This potential selection bias may lead us unable to exactly compare the susceptibility of various brain disorders to CCD. Another limitation was that the heterogeneity either among subgroups of a specific disease or within brain metabolic asymmetrical profile in each patient was not investigated. For the former, the magnitude of cerebellar AI would be higher in high-grade than in low-grade gliomas (Liu et al., 2018; Otte et al., 1998). For the latter, applications of radiomics and artificial intelligence approaches could provide further interpretation of metabolic asymmetrical profile by extracting and analyzing the high dimensional data. Moreover, 8 epilepsy patients in our study showed neither CCH nor conventional CCD. In addition to the lowest total volume of supratentorial metabolic abnormalities, the roughly symmetrical cerebellar metabolism may also be attributed to the ^{18}F-FDG PET imaging performed during subclinical seizure episode, rather than ictal state or status epilepticus. Despite these limitations, future research directions may be highlighted based on our preliminary results.

5. Conclusion

Voxel-based AI analysis has the potential to be served as a standard approach for assessing the asymmetrical profile of CCD in various brain disorders. Greater AI_{max}, lower AI_{min} and AI_{min} located at striatum & thalamus might be predisposing factors for CCD in patients with unilateral supratentorial hypermetabolic lesions. Relative increased activities in contralateral SMC and PrG could be a compensatory mechanism for the CCD associated abnormal brain network.

Ethical approval

The study protocol was approved by the Institutional Review Board of Tongji Hospital, Tongji Medical College, Huazhong University of Science and Technology, and the informed consent was waived.

Funding

This work was supported by the National Natural Science Foundation of China (NSFC) (grant number 81801729, 91959119 and 81873903).

CRediT authorship contribution statement

Yuankai Zhu: Conceptualization, Methodology, Software, Formal analysis, Investigation, Data curation, Writing – original draft, Visualization, Funding acquisition. **Ge Ruan:** Software, Validation, Investigation, Data curation, Writing – original draft, Visualization. **Sijuan Zou:** Validation, Investigation, Data curation, Writing – review & editing. **Zhaoting Cheng:** Validation, Investigation, Data curation, Writing – review & editing. **Xiaohua Zhu:** Conceptualization, Methodology, Formal analysis, Writing – review & editing, Visualization, Supervision, Project administration, Funding acquisition.

Declaration of Competing Interest

The authors declare that they have no known competing financial interests or personal relationships that could have appeared to influence the work reported in this paper.

References

Baron, J.C., Bousser, M.G., Comar, D., Castaigne, P., 1981. "Crossed cerebellar diaschisis" in human supratentorial brain infarction. Trans. Am. Neurol. Assoc. 105, 459–461.

Bonini, F., Burle, B., Liégeois-Chauvel, C., Régis, J., Chauvel, P., Vidal, F., 2014. Action monitoring and medial frontal cortex: leading role of supplementary motor area. Science 343, 888–891. https://doi.org/10.1126/science.1247412.

Bostan, A.C., Dum, R.P., Strick, P.L., 2010. The basal ganglia communicate with the cerebellum. Proc. Natl. Acad. Sci. 107, 8452–8456. https://doi.org/10.1073/pnas.1000496107.

Bostan, A.C., Dum, R.P., Strick, P.L., 2013. Cerebellar networks with the cerebral cortex and basal ganglia. Trends Cogn. Sci. 17, 241–254. https://doi.org/10.1016/j.tics.2013.03.003.

Calabria, F., Schillaci, O., 2012. Recurrent glioma and crossed cerebellar diaschisis in a patient examined with 18F-DOPA and 18F-FDG PET/CT. Clin. Nucl. Med. 37, 878–879. https://doi.org/10.1097/RLU.0b013e318262af2a.

Cavanna, A.E., Trimble, M.R., 2006. The precuneus: a review of its functional anatomy and behavioural correlates. Brain 129, 564–583. https://doi.org/10.1093/brain/awl004.

Chang, C.-C., Ku, C.-H., Chang, S.-T., 2017. Postural asymmetry correlated with lateralization of cerebellar perfusion in persons with chronic stroke: a role of crossed cerebellar diaschisis in left side. Brain Inj. 31, 90–97. https://doi.org/10.1080/02699052.2016.1210229.

Chen, S., Guan, M., Lian, H.-J., Ma, L.-J., Shang, J.-K., He, S., Ma, M.-M., Zhang, M.-L., Li, Z.-Y., Wang, M.-Y., Shi, D.-P., Zhang, J.-W., 2014. Crossed cerebellar diaschisis detected by arterial spin-labeled perfusion magnetic resonance imaging in subacute ischemic stroke. J. Stroke Cerebrovasc. Dis. 23, 2378–2383. https://doi.org/10.1016/j.jstrokecerebrovasdis.2014.05.009.

Cui, R., Niu, N., Li, F., 2014. Crossed cerebellar hypermetabolism demonstrated by FDG PET. Clin. Nucl. Med. 39, 409–412. https://doi.org/10.1097/rlu.0000000000000388.

Devita, M., Alberti, F., Fagnani, M., Masina, F., Ara, E., Sergi, G., Mapelli, D., Coin, A., 2021. Novel insights into the relationship between cerebellum and dementia: a narrative review as a toolkit for clinicians. Ageing Res. Rev. 70, 101389 https://doi.org/10.1016/j.arr.2021.101389.

Didelot, A., Mauguiere, F., Redoute, J., Bouvard, S., Lothe, A., Reilhac, A., Hammers, A., Costes, N., Ryvlin, P., 2010. Voxel-based analysis of asymmetry index maps increases the specificity of 18F-MPPF PET abnormalities for localizing the epileptogenic zone in temporal lobe epilepsies. J. Nucl. Med. 51, 1732–1739. https://doi.org/10.2967/jnumed.109.070938.

Diehl-Schmid, J., Licata, A., Goldhardt, O., Förstl, H., Yakushew, I., Otto, M., Anderl-Straub, S., Beer, A., Ludolph, A., Landwehrmeyer, G., Levin, J., Danek, A., Fliessbach, K., Spottke, A., Fassbender, K., Lyros, E., Prudlo, J., Krause, B., Volk, A., Edbauer, D., Schroeter, M., Drzezga, A., Kornhuber, J., Lauer, M., Grimmer, T., 2019. FDG-PET underscores the key role of the thalamus in frontotemporal lobar degeneration caused by C9ORF72 mutations. Transl. Psychiatry 9, 54. https://doi.org/10.1038/s41398-019-0381-1.

Eidelberg, D., 2009. Metabolic brain networks in neurodegenerative disorders: a functional imaging approach. Trends Neurosci. 32, 548–557. https://doi.org/10.1016/j.tins.2009.06.003.

Franceschi, A.M., Clifton, M.A., Naser-Tavakolian, K., Ahmed, O., Bangiyev, L., Clouston, S., Franceschi, D., 2021. FDG PET/MRI for visual detection of crossed cerebellar diaschisis in patients with dementia. Am. J. Roentgenol. 216, 165–171. https://doi.org/10.2214/ajr.19.22617.

Goldwaser, E.L., Edwards, S., Ajith, A., Nagele, E., Elliker, J., Ferris, M., Thompson, S.J., 2020. First reported case of anti-N-methyl d-aspartate receptor encephalitis in a child with crossed cerebellar diaschisis and extreme delta brush. Psychosomatics 61, 840–845. https://doi.org/10.1016/j.psym.2019.12.003.

Graffeo, C.S., Snyder, K.A., Nasr, D.M., Murphy, M.E., Carr, C.M., Hocker, S.E., 2016. Prognostic and mechanistic factors characterizing seizure-associated crossed cerebellar diaschisis. Neurocrit. Care 24, 258–263. https://doi.org/10.1007/s12028-015-0155-4.

Griffiths, P.D., Boodram, M.B., Blaser, S., Armstrong, D., Gilday, D.L., Harwood-Nash, D., 1997. 99mTechnetium HMPAO imaging in children with the Sturge-Weber syndrome: a study of nine cases with CT and MRI correlation. Neuroradiology 39, 219–224. https://doi.org/10.1007/s002340050398.

Hamaide, J., Lukacova, K., Van Audekerke, J., Verhoye, M., Kubikova, L., Van der Linden, A., 2018. Neuroplasticity in the cerebello-thalamo-basal ganglia pathway: a longitudinal in vivo MRI study in male songbirds. Neuroimage 181, 190–202. https://doi.org/10.1016/j.neuroimage.2018.07.010.

Hertel, A., Wenz, H., Al-Zghloul, M., Hausner, L., FrÖLich, L., Groden, C., FÖRster, A.,, 2021. Crossed cerebellar diaschisis in Alzheimer's disease detected by arterial spin-labelling perfusion MRI. In vivo (Athens, Greece) 35, 1177–1183. https://doi.org/10.21873/invivo.12366.

Hirata, K., Hattori, N., Takeuchi, W., Shiga, T., Morimoto, Y., Umegaki, K., Kobayashi, K., Manabe, O., Okamoto, S., Tamaki, N., 2015. Metabolic activity of red nucleus and its correlation with cerebral cortex and cerebellum: a study using a high-resolution semiconductor PET system. J. Nucl. Med. 56, 1206–1211. https://doi.org/10.2967/jnumed.114.152504.

Hokari, M., Kuroda, S., Simoda, Y., Uchino, H., Hirata, K., Shiga, T., Nakayama, N., Houkin, K., Tamaki, N., 2012. Transient crossed cerebellar diaschisis due to cerebral hyperperfusion following surgical revascularization for moyamoya disease: case report. Neurol. Med. Chir. (Tokyo) 52, 350–353. https://doi.org/10.2176/nmc.52.350.

Hoshi, E., Tremblay, L., Féger, J., Carras, P.L., Strick, P.L., 2005. The cerebellum communicates with the basal ganglia. Nat. Neurosci. 8, 1491–1493. https://doi.org/10.1038/nn1544.

Hou, Y., Guo, K., Fan, X., Shang, K., Wang, J., Wang, Z., Shan, Y., Zhao, G., Lu, J., 2021. Crossed cerebellar diaschisis: risk factors and prognostic value in focal cortical dysplasia by (18)F-FDG PET/CT. Ann. Nucl. Med. 35, 719–727. https://doi.org/10.1007/s12149-021-01613-8.

Hsieh, T.-Y., Liu, C.-C., He, H.-C., Cheng, Y.-Y., Chang, S.-T., 2020. Persistence of glenohumeral subluxation is correlated with prolonged existence of crossed cerebellar diaschisis in a hemiplegic stroke survivor: a pilot study. Gerontol. Geriatr. Res. 2, 1–6. https://doi.org/10.31487/j.GGR.2020.02.09.

Inatomi, Y., Nakajima, M., Yonehara, T., 2021. Aphasia induced by infratentorial ischemic stroke: two case reports. Cogn. Behav. Neurol. 34, 129–139. https://doi.org/10.1097/wnn.0000000000000266.

Joswig, H., Surbeck, W., Scholtes, F., Bratelj, D., Hildebrandt, G., 2021. The debate on apraxia and the supplementary motor area in the twentieth century. Acta Neurochir. 163, 1247–1255. https://doi.org/10.1007/s00701-020-04509-0.

Kang, K.M., Sohn, C.H., Choi, S.H., Jung, K.H., Yoo, R.E., Yun, T.J., Kim, J.H., Park, S.W., 2017. Detection of crossed cerebellar diaschisis in hyperacute ischemic stroke using arterial spin-labeled MR imaging. PLoS One 12, e0173971. https://doi.org/10.1371/journal.pone.0173971.

Kang, K.M., Sohn, C.H., Kim, B.S., Kim, Y.I., Choi, S.H., Yun, T.J., Kim, J.H., Park, S.W., Cheon, G.J., Han, M.H., 2015. Correlation of asymmetry indices measured by arterial spin-labeling MR imaging and SPECT in patients with crossed cerebellar diaschisis. Am. J. Neuroradiol. 36, 1662–1668. https://doi.org/10.3174/ajnr.A4366.

Kawabata, K., Watanabe, H., Bagarinao, E., Ohdake, R., Hara, K., Ogura, A., Masuda, M., Kato, T., Tsuboi, T., Maesawa, S., Katsuno, M., Sobue, G., 2020. Cerebello-basal ganglia connectivity fingerprints related to motor/cognitive performance in Parkinson's disease. Parkinsonism Relat. Disord. 80, 21–27. https://doi.org/10.1016/j.parkreldis.2020.09.005.

Kawai, N., Kawanishi, M., Tamiya, T., Nagao, S., 2005. Crossed cerebellar glucose hypermetabolism demonstrated using PET in symptomatic epilepsy–case report. Ann. Nucl. Med. 19, 231–234. https://doi.org/10.1007/bf02984610.

Koy, A., Klee, D., Weber, A.A., Karenfort, M., Mayatepek, E., 2012. Crossed cerebellar diaschisis after status epilepticus in a young child. Neuropediatrics 43, 55–58. https://doi.org/10.1055/s-0032-1309306.

Kurth, F., Gaser, C., Luders, E., 2015. A 12-step user guide for analyzing voxel-wise gray matter asymmetries in statistical parametric mapping (SPM). Nat. Protoc. 10, 293–304. https://doi.org/10.1038/nprot.2015.014.

Kurthen, M., Reichmann, K., Linke, D.B., Biersack, H.J., Reuter, B.M., Durwen, H.F., Grünwald, F., 1990. Crossed cerebellar diaschisis in intracarotid sodium amytal procedures: a SPECT study. Acta Neurol. Scand. 81, 416–422. https://doi.org/10.1111/j.1600-0404.1990.tb00987.x.

Kwon, Y.C., Kim, J.H., Ahn, T.B., 2015. Ataxia of cortical origin via crossed cerebellar diaschisis. Neurol. Sci. 36, 161–163. https://doi.org/10.1007/s10072-014-1846-x.

Lee, T.-H., Huang, K.-L., Chang, T.-Y., Ho, M.-Y., Wey, S.-P., Hsieh, C.-J., Yen, T.-C., Lin, K.-J., Hsiao, I.-T., 2017. Early-phase 18F-AV-45 PET imaging can detect crossed cerebellar diaschisis following carotid artery stenosis and cerebral hypoperfusion. Curr. Neurovasc. Res. 14, 258–265. https://doi.org/10.2174/1567202614666170621102101.

Leisman, G., Melillo, R., 2013. The basal ganglia: motor and cognitive relationships in a clinical neurobehavioral context. Rev. Neurosci. 24, 9–25. https://doi.org/10.1515/revneuro-2012-0067.

Lin, T., Lyu, Y., Qu, J., Cheng, X., Fan, X., Zhang, Y., Hou, B., You, H., Ma, W., Feng, F., 2018. Crossed cerebellar diaschisis in post-treatment glioma patients: a comparative study of arterial spin labelling and dynamic susceptibility contrast. Eur. J. Radiol. 107, 70–75. https://doi.org/10.1016/j.ejrad.2018.08.001.

Lindegaard, M.W., Skretting, A., Hager, B., Watne, K., Lindegaard, K.F., 1986. Cerebral and cerebellar uptake of 99mTc-(d,1)-hexamethyl-propyleneamine oxime (HM-PAO) in patients with brain tumor studied by single photon emission computerized tomography. Eur. J. Nucl. Med. 12, 417–420. https://doi.org/10.1007/bf00254743.

Liu, X., Li, J., Xu, Q., Mantini, D., Wang, P., Xie, Y., Weng, Y., Ma, C., Sun, K., Zhang, Z., Lu, G., 2018. Pathological factors contributing to crossed cerebellar diaschisis in cerebral gliomas: a study combining perfusion, diffusion, and structural MR imaging. Neuroradiology 60, 643–650. https://doi.org/10.1007/s00234-018-2015-3.

Ma, J., Zhao, L., Yuan, K., Yan, J., Zhang, Y., Zhu, J., Yan, C., 2022. Crossed cerebellar diaschisis after acute ischemic stroke detected by intravoxel incoherent motion magnetic resonance imaging. Neurol. Sci. 43, 1135–1141. https://doi.org/10.1007/s10072-021-05425-6.

Ma, Y., Tang, C., Spetsieris, P.G., Dhawan, V., Eidelberg, D., 2007. Abnormal metabolic network activity in Parkinson's disease: Test—Retest reproducibility. J. Cereb. Blood Flow Metab. 27, 597–605. https://doi.org/10.1038/sj.jcbfm.9600358.

McGettigan, C., Walsh, E., Jessop, R., Agnew, Z.K., Sauter, D.A., Warren, J.E., Scott, S.K., 2013. Individual differences in laughter perception reveal roles for mentalizing and sensorimotor systems in the evaluation of emotional authenticity. Cereb. Cortex 25, 246–257. https://doi.org/10.1093/cercor/bht227.

Nelissen, N., Van Paesschen, W., Baete, K., Van Laere, K., Palmini, A., Van Billoen, H., Dupont, P., 2006. Correlations of interictal FDG-PET metabolism and ictal SPECT perfusion changes in human temporal lobe epilepsy with hippocampal sclerosis. Neuroimage 32, 684–695. https://doi.org/10.1016/j.neuroimage.2006.04.185.

Nishida, Y., Hizume, M., Fumimura, Y., Ichikawa, T., 2019. Cerebellar cognitive affective syndrome improved by donepezil. Intern. Med. 58, 1003–1006. https://doi.org/10.2169/internalmedicine.1206-18.

Nocuń, A., Wojczal, J., Szczepańska-Szerej, H., Wilczyński, M., Chrapko, B., 2013. Quantitative evaluation of crossed cerebellar diaschisis, using voxel-based analysis of Tc-99m ECD brain SPECT. Nucl. Med. Rev. Cent East Eur. 16, 31–34. https://doi.org/10.5603/nmr.2013.0006.

Noguchi, T., Nishihara, M., Egashira, Y., Azama, S., Hirai, T., Kitano, I., Yakushiji, Y., Kawashima, M., Irie, H., 2015. Arterial spin-labeling MR imaging of cerebral hemorrhages. Neuroradiology 57, 1135–1144. https://doi.org/10.1007/s00234-015-1574-9.

Otte, A., Roelcke, U., von Ammon, K., Hausmann, O., Maguire, R.P., Missimer, J., Müller-Brand, J., Radü, E.W., Leenders, K.L., 1998. Crossed cerebellar diaschisis and brain tumor biochemistry studied with positron emission tomography, [18F] fluorodeoxyglucose and [11C]methionine. J. Neurol. Sci. 156, 73–77. https://doi.org/10.1016/s0022-510x(98)00019-7.

Palesi, F., De Rinaldis, A., Castellazzi, G., Calamante, F., Muhlert, N., Chard, D., Tournier, J.D., Magenes, G., D'Angelo, E., Gandini Wheeler-Kingshott, C.A.M., 2017. Contralateral cortico-ponto-cerebellar pathways reconstruction in humans in vivo: implications for reciprocal cerebro-cerebellar structural connectivity in motor and non-motor areas. Sci. Rep. 7, 12841. https://doi.org/10.1038/s41598-017-13079-8.

Park, C.H., Kim, S.M., Streletz, L.J., Zhang, J., Intenzo, C., 1992. Reverse crossed cerebellar diaschisis in partial complex seizures related to herpes simplex encephalitis. Clin. Nucl. Med. 17, 732–735. https://doi.org/10.1097/00003072-199209000-00011.

Provost, K., La Joie, R., Strom, A., Iaccarino, L., Edwards, L., Mellinger, T.J., Pham, J., Baker, S.L., Miller, B.L., Jagust, W.J., Rabinovici, G.D., 2021. Crossed cerebellar diaschisis on 18F-FDG PET: frequency across neurodegenerative syndromes and association with 11C-PIB and 18F-Flortaucipir. J. Cereb. Blood Flow Metab. 41, 2329–2343. https://doi.org/10.1177/0271678x211001216.

Reesink, F.E., García, D.V., Sánchez-Catasús, C.A., Peretti, D.E., Willemsen, A.T., Boellaard, R., Meles, S.K., Huitema, R.B., de Jong, B.M., Dierckx, R.A., De Deyn, P.P., 2018. Crossed cerebellar diaschisis in Alzheimer's disease. Curr. Alzheimer Res. 15, 1267–1275. https://doi.org/10.2174/1567205015666180913102615.

Savic, I., Altshuler, L., Passaro, E., Baxter, L., Engel Jr., J., 1996. Localized cerebellar hypometabolism in patients with complex partial seizures. Epilepsia 37, 781–787. https://doi.org/10.1111/j.1528-1157.1996.tb00652.x.

Schindlbeck, K.A., Lucas-Jiménez, O., Tang, C.C., Morbelli, S., Arnaldi, D., Pardini, M., Pagani, M., Ibarretxe-Bilbao, N., Ojeda, N., Nobili, F., Eidelberg, D., 2020. Metabolic network abnormalities in drug-naïve Parkinson's disease. Mov. Disord. 35, 587–594. https://doi.org/10.1002/mds.27960.

Sebök, M., van Niftrik, C.H.B., Halter, M., Hiller, A., Seystahl, K., Pangalu, A., Weller, M., Stippich, C., Regli, L., Fierstra, J., 2020. Crossed cerebellar diaschisis in patients with diffuse glioma is associated with impaired supratentorial cerebrovascular reactivity and worse clinical outcome. Cerebellum 19, 824–832. https://doi.org/10.1007/s12311-020-01174-y.

Sebök, M., van Niftrik, C.H.B., Piccirelli, M., Muscas, G., Pangalu, A., Wegener, S., Stippich, C., Regli, L., Fierstra, J., 2021. Crossed cerebellar diaschisis in patients with symptomatic unilateral anterior circulation stroke is associated with hemodynamic impairment in the ipsilateral MCA territory. J. Magn. Reson. Imaging 53, 1190–1197. https://doi.org/10.1002/jmri.27410.

Sin, D.S., Kim, M.H., Park, S.-A., Joo, M.C., Kim, M.S., 2018. Crossed cerebellar diaschisis: risk factors and correlation to functional recovery in intracerebral hemorrhage. Ann. Rehabil. Med. 42, 8. https://doi.org/10.5535/arm.2018.42.1.8.

Sjöberg, R.L., Stålnacke, M., Andersson, M., Eriksson, J., 2019. The supplementary motor area syndrome and cognitive control. Neuropsychologia 129, 141–145. https://doi.org/10.1016/j.neuropsychologia.2019.03.013.

Sommer, W.H., Bollwein, C., Thierfelder, K.M., Baumann, A., Janssen, H., Ertl-Wagner, B., Reiser, M.F., Plate, A., Straube, A., von Baumgarten, L., 2016. Crossed cerebellar diaschisis in patients with acute middle cerebral artery infarction: occurrence and perfusion characteristics. J. Cereb. Blood Flow Metab. 36, 743–754. https://doi.org/10.1177/0271678x15617953.

Takahashi, S., Horiguchi, T., 2020. Relationship between ischaemic symptoms during the early postoperative period in patients with moyamoya disease and changes in the cerebellar asymmetry index. Clin. Neurol. Neurosurg. 197, 106090 https://doi.org/10.1016/j.clineuro.2020.106090.

Teoh, E.J., Green, A.L., Bradley, K.M., 2014. Crossed cerebellar diaschisis due to cerebral diffuse large B cell lymphoma on 18F-FDG PET/CT. Int. J. Hematol. 100, 415–416. https://doi.org/10.1007/s12185-014-1656-1.

Thibes, R.B., Novaes, N.P., Lucato, L.T., Campanholo, K.R., Melo, L.M., Leite, C.C., Amaro, E., Barbosa, E.R., Bor-Seng-Shu, E., Cardoso, E.F., Sato, J.R., 2017. Altered functional connectivity between precuneus and motor systems in Parkinson's disease patients. Brain Connect. 7 (10), 643–647.

Uchino, H., Kazumata, K., Ito, M., Nakayama, N., Kuroda, S., Houkin, K., 2021. Crossed cerebellar diaschisis as an indicator of severe cerebral hyperperfusion after direct bypass for moyamoya disease. Neurosurg. Rev. 44, 599–605. https://doi.org/10.1007/s10143-020-01265-8.

Umemura, A., Suzuka, T., 2000. Crossed cerebellar hyperperfusion in symptomatic epilepsy–two case reports. Neurol. Med. Chir. (Tokyo) 40, 65–68. https://doi.org/10.2176/nmc.40.65.

von Bieberstein, L., van Niftrik, C.H.B., Sebök, M., El Amki, M., Piccirelli, M., Stippich, C., Regli, L., Luft, A.R., Fierstra, J., Wegener, S., 2021. Crossed cerebellar diaschisis indicates hemodynamic compromise in ischemic stroke patients. Transl. Stroke Res. 12, 39–48. https://doi.org/10.1007/s12975-020-00821-0.

Vyas, S., Bhatia, V., Dass, G., Sankhyan, N., 2019. Macroscopic and microscopic perfusion changes in hemispheric status epilepticus with cross cerebellar diaschisis. J. Pediatr. Neurosci. 14, 55. https://doi.org/10.4103/jpn.JPN_65_18.

Wang, H., Tian, Y., Liu, Y., Chen, Z., Zhai, H., Zhuang, M., Zhang, N., Jiang, Y., Gao, Y., Feng, H., Zhang, Y., 2021. Population-specific brain [18F]-FDG PET templates of Chinese subjects for statistical parametric mapping. Sci. Data 8, 305. https://doi.org/10.1038/s41597-021-01089-1.

Wang, J., Pan, L.-J., Zhou, B., Zu, J.-Y., Zhao, Y.-X., Li, Y., Zhu, W.-Q., Li, L., Xu, J.-R., Chen, Z.-A., 2020. Crossed cerebellar diaschisis after stroke detected noninvasively by arterial spin-labeling MR imaging. BMC Neurosci. 21, 46. https://doi.org/10.1186/s12868-020-00595-z.

Won, J., Choi, D.S., Hong, S.J., Shin, H.S., Baek, H.J., Choi, H.C., Kim, M., Kim, R.B., 2018. Crossed cerebellar hyperperfusion in patients with seizure-related cerebral cortical lesions: an evaluation with arterial spin labelling perfusion MR imaging. Radiol. Med. 123, 843–850. https://doi.org/10.1007/s11547-018-0921-4.

Yajima, R., Naruse, S., 2021. Corticobasal syndrome with supplementary motor area aphasia. Intern. Med. 60, 1799–1800. https://doi.org/10.2169/internalmedicine.6212-20.

Yokota, H., Ida, Y., 2019. Crossed cerebellar diaschisis in status epilepticus. Neurochirurgie 65, 425–426. https://doi.org/10.1016/j.neuchi.2019.08.001.

Yoshida, J., Komoribayashi, N., Oikawa, K., Ohmama, S., Kojima, D., Shimada, Y., Ogasawara, K., 2018. ¹²³I-Iomazenil Single-photon emission computed tomography imaging in a patient with mild traumatic subdural hematoma accompanied by delayed transient aphasia. No Shinkei Geka 46, 1081–1086. https://doi.org/10.11477/mf.1436203872.

Zhang, M., Cao, Y., Wu, F., Zhao, C., Ma, Q., Li, K., Lu, J., 2019. Characteristics of cerebral perfusion and diffusion associated with crossed cerebellar diaschisis after acute ischemic stroke. Jpn. J. Radiol. 38, 126–134. https://doi.org/10.1007/s11604-019-00898-0.

Zhu, Y., Feng, J., Ji, J., Hou, H., Chen, L., Wu, S., Liu, Q., Yao, Q., Du, P., Zhang, K., Chen, Q., Chen, Z., Zhang, H., Tian, M., 2017. Alteration of monoamine receptor activity and glucose metabolism in pediatric patients with anticonvulsant-induced cognitive impairment. J. Nucl. Med. 58, 1490–1497. https://doi.org/10.2967/jnumed.116.189290.